JOURNAL OF GEOPHYSICAL RESEARCH, VOL. 112, B06310, doi:10.1029/2006JB004552, 2007

Illuminating the plate interface structure beneath Cook Strait, New Zealand, with receiver functions

Oliver S. Boyd,[1] Martha K. Savage,[2] Anne F. Sheehan,[1] and Craig H. Jones[1]

Received 8 June 2006; revised 27 January 2007; accepted 26 March 2007; published 27 June 2007.

[1] Using teleseismic receiver functions derived from broadband seismic arrays on the north end of the South Island and south end of the North Island of New Zealand, we image seismic impedance discontinuities in the upper mantle beneath Cook Strait using common conversion point (CCP) and Kirchhoff migration methods. Our primary findings are observations of discontinuities associated with the top of the subducting Pacific Plate. Our results suggest that contrary to recent suggestions, the plate is continuous under the northern South Island through the region of seismicity deeper than 50 km. West of Cook Strait, the slab dips steeply to the northwest. We find evidence for a low-velocity layer at the top of the slab, near which much of the seismicity is concentrated. We see hints of two crustal discontinuities, consistent with observations from previous studies. We also see substantial and continuous energy on the transverse receiver function stacks above the mantle wedge extending to the northwestern edge of our stacks, which may indicate seismic anisotropy above 50 km depth.

Citation: Boyd, O. S., M. K. Savage, A. F. Sheehan, and C. H. Jones (2007), Illuminating the plate interface structure beneath Cook Strait, New Zealand, with receiver functions, *J. Geophys. Res.*, *112*, B06310, doi:10.1029/2006JB004552.

1. Introduction

[2] The northern South Island of New Zealand presents an excellent opportunity to study subduction zone structure in a region where subduction gives way to an oblique transform boundary [*Cande and Stock*, 2004]. The Pacific Plate subducts beneath the Australian plate on the North Island and northernmost South Island while the Australian plate subducts beneath the far southern portion of the South Island. The Alpine Fault on the South Island bridges the two subduction zones and is an oblique dextral strike-slip fault separating the Pacific and Australian plates. The islands are marked with various natural hazards due to this complex plate boundary from volcanic on the North Island to seismic throughout.

[3] Patterns of seismicity in the northern subduction zone suggest a strongly bending plate that approaches a near-vertical orientation at 200 km depth [*Anderson and Webb*, 1994]. Focal mechanisms indicate (1) compression and thrust faulting in the overlying crust resulting from strong coupling between the two plates and (2) downdip tension in the subducting plate beneath about 50 km depth [*Reyners et al.*, 1997]. Deeper seismicity, >100 km depth, has an abrupt southern edge west of Nelson (Figure 1), which may reflect a termination of the subducting plate [*Furlong*, 2004]. However, focal mechanisms do not change at this location, and so some authors argue that the subducting plate continues to the southwest toward Westport albeit without sufficient stress to cause seismicity [*Reyners and Robertson*, 2004]. In the transform region of the South Island, the shallower seismicity at 30 to 100 km depth is suggested to be due to high shear strain and depressed geotherms [*Kohler and Eberhart-Phillips*, 2003].

[4] Various investigations have been performed to elucidate the finer structure of the crust and uppermost mantle [*Savage*, 1998; *Savage et al.*, 2007; *Wilson et al.*, 2004]. In an attempt to explain *ScSp* precursors (shear waves that reflect off of the core and then convert to a *P* wave near the Earth's surface) observed in the southern North Island, *Bourne and Stuart* [2000] inferred the presence of a low-velocity layer at the top of the subducting slab, which they think is caused by subducted sediments. This covers a thick oceanic crust which increases in thickness to the southwest from 11 km near the Tararua broadband array (TBA) to 27 km in the onshore section of the Chatham Rise at the southeastern section of our study region [*Bourne and Stuart*, 2000; *Eberhart-Phillips and Reyners*, 1997; *Reyners and Cowan*, 1993]. Receiver functions from station SNZO on the North Island suggest that these sediments are anisotropic [*Savage*, 1998; *Savage et al.*, 2007]. On the north end of the South Island, *Wilson et al.* [2004] found an anisotropic lower crustal layer and inferred distributed deformation in the lower crust between the Australian and Pacific plates.

[5] Regional tomographic studies of the upper mantle beneath New Zealand have been performed [*Eberhart-*

[1]Department of Geological Sciences, University of Colorado at Boulder, Boulder, Colorado, USA.
[2]Institute of Geophysics, School of Earth Sciences, Victoria University of Wellington, Wellington, New Zealand.

0148-0227/07/2006JB004552$09.00

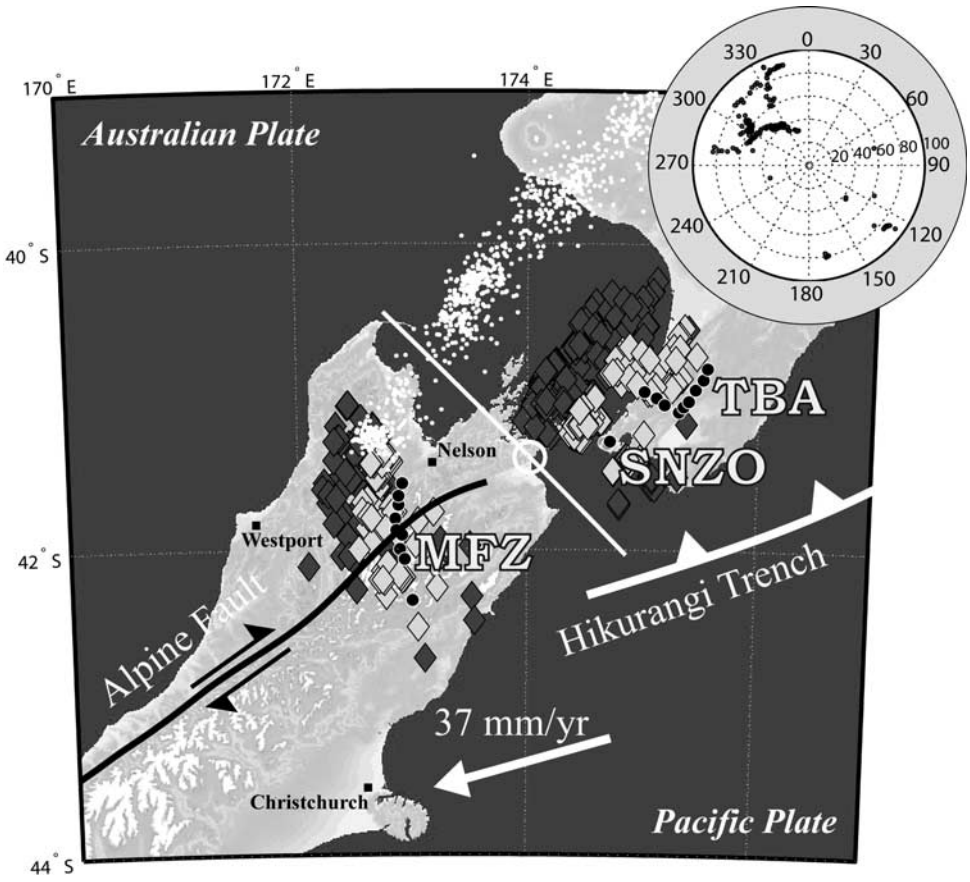

Figure 1. Map of New Zealand with locations of the Tararua broadband array (TBA), SNZO, and Marlborough seismic study (MFZ) (filled black circles). The North and South islands are separated by Cook Strait. The Pacific Plate moves SW relative to the Australian Plate at 37 mm/yr and subducts beneath the North Island at the Hikurangi Trench. The dextral Alpine fault separates the two plates along much of the South Island. The white line that trends NW is the location of the profiles in Figures 3 and 4. The white circle is the center of the grid corresponding to $X = 0$. The dark (light) diamonds are piercing points of seismic rays at 200 (100) km depth for our data set. The white dots are earthquakes from greater than 150 km depth and give some idea of the northwestern and southwestern extent of the subducting plate. The polar figure in the upper right shows the distribution of azimuths and distances for the teleseismic events in this study.

Phillips and Reyners, 1997; *Kohler and Eberhart-Phillips*, 2002; *Stern et al.*, 2000] and indicate the presence of relatively high seismic velocities in the mantle lithosphere, presumably the result of relatively cold and dense material descending into the surrounding mantle as might occur from the subducting Pacific Plate. However, the images produced from these studies are characterized by moderately amorphous increases in seismic velocities. They lack the precision to identify seismic discontinuities and cannot distinguish the difference between whether the Pacific Plate continues to subduct beneath the northern South Island or whether the plates simply thicken as a result of convergence [*Stern et al.*, 2000].

[6] We seek to more precisely image and better interpret the subsurface structure along a northwest-southeast transect between the North and South islands of New Zealand. We accomplish this goal by producing common conversion point and migrated stacks of teleseismic receiver functions, calculated from data recorded by permanent and temporary seismic networks in the southern North Island and northern South Island of New Zealand.

2. Method

[7] This study combines the data from several broadband seismic arrays on either side of Cook Strait, New Zealand (Figure 1). On the North Island, TBA acquired data from February 1991 to July 1992 and consists of nine broadband seismometers [*Stuart et al.*, 1995]. The broadband Incorporated Research Institutions for Seismology (IRIS) station SNZO has been continuously recording since March 1992 and was supplemented with four additional broadband seismometers during most of 1998 [*Stewart*, 1998]. The Marlborough seismic study (MFZ) on the South Island was active from October 2000 to May 2002 and utilized nine broadband seismometers in addition to 45 short-period seismometers [*Wilson et al.*, 2001, 2004]. Many local and teleseismic events have been recorded with these arrays. For

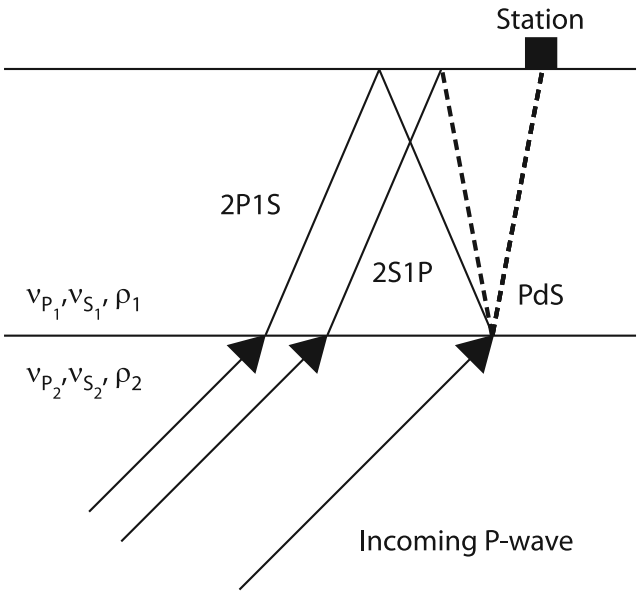

Figure 2. Schematic representation of how a receiver function is produced by subsurface impedance contrasts. Solid (dashed) lines are *P* (*S*) waves. The incoming *P* wave will generate reflected and refracted *P* and S waves. The refracted *S* wave, P_dS, is of primary interest while the refracted *P* wave will generate free-surface multiples 2S1P and 2P1S.

this study, over 100 earthquakes between 30° and 90° epicentral distance with a body wave magnitude $\geq$5 were recorded, yielding 275 broadband traces from which to make and interpret receiver functions. Some 197 of these are from North Island stations while the rest are from South Island stations. The distribution of back azimuths is limited (Figure 1). Most hail from the northwest. There are several events used from the southeast and one each from the southwest and northeast. No azimuthal weighting was used, and we expect minimal influence of southeasterly azimuths on the illumination of the subducting slab.

[8] A receiver function is ideally a time series consisting of arrivals that represent the subsurface seismic impedance contrasts. It is most sensitive to shear wave speed discontinuities but also has a slight dependence on *P* wave speed and density discontinuities. A *P* wave that impinges from below and encounters a seismic impedance contrast will generate reflected and transmitted *P* and *S* waves. For horizontal subsurface impedance contrasts, the transmitted *P* wave will appear primarily on the vertical component of motion, whereas the transmitted *S* waves generated from each subsurface discontinuity will appear primarily on the radial component of motion. We can then deconvolve the vertical component from the radial to remove the complex source time function and instrument response and obtain a series of arrivals corresponding to the subsurface seismic impedance contrasts. The resulting time series is termed as a radial receiver function [*Langston*, 1977]. The vertical component seismogram can also be deconvolved from the transverse component of motion resulting in a transverse receiver function. For flat isotropic media, the transverse receiver function should be zero. Dipping isotropic media will produce arrivals on the transverse receiver function that will coincide with arrivals on the radial receiver function. Azimuthally anisotropic media splits a transmitted *S* wave, assuming the incoming *S* wave is not polarized along the fast or slow axes. This will generate two positive amplitude arrivals on the radial component of motion and a set of equal and opposite polarity arrivals on the transverse. Unfortunately, free-surface multiples, also referred to as reverberations, also appear in and contaminate the receiver functions (Figure 2).

[9] Deconvolution can be performed in the frequency domain [*Dueker and Sheehan*, 1998] or in the time domain [*Ligorria and Ammon*, 1999]. We decided to employ the iterative time domain deconvolution [*Ligorria and Ammon*, 1999] because, when evaluating ray parameter plots, this technique produced the most coherent receiver functions. With this method, the vertical component of the broadband seismometer is iteratively correlated and subtracted from the radial, revealing various types of multiples as well as *P* to *S* conversions from subsurface seismic discontinuities. The *P* to *S* conversions, P_dS, where d represents the subsurface position of a *P* wave impedance contrast, are of primary interest. To remove unwanted high-frequency noise, the resulting receiver functions are filtered by convolution with a Gaussian wavelet having a standard deviation of $\sim$0.2 s [*Yilmaz*, 2001].

[10] We produce subsurface images of the seismic discontinuities using common conversion point (CCP) stacking of the receiver functions [*Dueker and Sheehan*, 1998] and two-dimensional Kirchhoff migration [*Sheehan et al.*, 2000]. The CCP stacking technique is analogous to the common midpoint (CMP) or common depth point (CDP) techniques used in reflection seismology. Stacking of receiver functions enhances coherent P_dS conversions while decreasing random noise and reducing the amplitudes of free-surface multiples. Seismic rays are traced from the station toward the event using the one-dimensional velocity model IASPEI91 [*Kennett and Engdahl*, 1991], and the receiver function is stretched along this raypath, corrected from time to distance using this one-dimensional velocity profile. The minor variations between IASPEI91 and other established one-dimensional velocity profiles [*Bourne and Stuart*, 2000; *Robinson*, 1986] make little difference in the resulting receiver function stacks [*Chen et al.*, 2005]. Our results and conclusions would be nearly unaffected by using a three-dimensional velocity model such as that produced by *Eberhart-Phillips and Reyners* [1997] since, for this region, velocity variations in these models are typically less than 5%. At 40 km depth, such a velocity anomaly, if held constant at all depths above 40 km, could move a discontinuity up or down 2 km, which is similar to or less than the likely uncertainty associated with the depths of our imaged discontinuities. A two-dimensional grid of subsurface bins, 1 km wide $\times$ 1 km deep extending to 150 km depth, is then defined (Figure 1), where the amplitudes for all receiver functions that pierce a given subsurface bin are averaged. Finally, each subsurface bin is laterally averaged with all bins within 5 km.

[11] Our implementation of two-dimensional Kirchhoff migration is a type of backprojection method in which each subsurface point is considered to be a scatterer or a point source. The traveltime between the arrival of the primary *P* wave and the *P* to *S* conversion due to this scatterer for all of the stations is calculated. The receiver function amplitudes

for all of the stations at these times are summed, and the result is placed at the location of the scatterer. Corrections are made to the amplitudes, before summation, for geometrical spreading, the amplitude dependence on incidence angle, termed as obliquity, and the polarity, in which the sign of the arrival changes depending on the angle of the scatterer-receiver raypath relative to the undisturbed incidence angle.

[12] The migration method used here differs from that of *Sheehan et al.* [2000] in the calculation of time on the receiver function trace for a given subsurface point. In their method, the arrival time for the *P* wave is calculated based on a radial earth model. The arrival time for the *P-SV* converted wave is calculated in a similar manner; a one-dimensional profile is used for the *P* wave traveltime from source to scatterer and for the converted *SV* wave traveltime from scatterer to station. The difference between the arrival times of the direct *P* and scattered *P-SV* is used to find the amplitude in the receiver function. This method is exact for subsurface structure without dip.

[13] For subsurface structure with nonzero dip, the direct *P* wave will come from a position closer to the scatterer that generated the *S* wave than would be inferred from the *P* wave raypath resulting from a one-dimensional earth structure. Yet since the subsurface velocity structure and the dip of the impedance contrasts are unknown a priori, the true direct *P* wave raypath is also not known. We have opted to simplify our calculation by assuming that the *P* and *S* waves travel directly from the scatterer to the station along straight raypaths through a one-dimensional velocity model [*Kennett and Engdahl*, 1991]. This assumption has greater validity as the subsurface structure increases in dip and is acceptable for flat-lying structure as can be seen by noting that the depth of the flat-lying 35-km synthetic discontinuity in Figure 4c lies close to 35 km depth. A more significant advantage is the improved computational efficiency of our method, requiring far less time to calculate the time difference between the direct *P* wave and converted *P-SV* wave. For a one-dimensional velocity profile and unbent raypaths, the time on the receiver function corresponding to the location of the scatterer is simply

$$t = \frac{D}{k} \sum_{z=1}^{k} \left(\frac{1}{v_{S_z}} - \frac{1}{v_{P_z}} \right) \tag{1}$$

where D is the distance between scatterer and station, k corresponds to the depth of interest, and v_S and v_P are the shear and *P* wave speeds, respectively, along this path.

[14] Additional difficulties that we overcame in the migration were the disproportionate number of receiver functions per station and the uneven spatial distribution of stations [*Bostock et al.*, 2001]. Before stacking, the individual receiver function amplitudes at each station are divided by the number of receiver functions present for that station. To account for the spatial distribution, a smooth histogram of station locations is created, having a correlation length of 20 km. The amplitudes are then further divided by the value of this function at the station location.

3. Results

[15] In our analysis, we must be sure that we can combine the North and South Island data sets in a northwest-southeast cross section. One strong argument for being able to combine the data sets is that the distribution of seismicity [*Anderson and Webb*, 1994] and the results from tomography [*Eberhart-Phillips and Henderson*, 2004; *Eberhart-Phillips and Reyners*, 1997] have a predominantly two-dimensional structure, which is perpendicular to our cross section. But given that the North and South Island stations are separated by a significant distance in the northeast-southwest direction and that the South Island stations tend to have a much lower signal-to-noise ratio due partly to the relatively short period of time over which they were deployed, we compare the North and South Island data sets to see if arrivals are continuous across the data sets. In Figure 3a, the stations to the southeast of $X = 0$ km are North Island stations while those northwest of $X = 0$ km are South Island stations. A line drawn from $X = 0$ km, $Z = 0$ km at the top of the stack to $X = 35$ km, $Z = 150$ km at the bottom roughly demarcates the two data sets. Nearly every arrival that is seen on the left side of this line can be traversed to the right. This observation lends credence to our being able to interpret features by combining both data sets even though we recognize that an apparent jump in the slab arrival, discussed below, might be caused partially by a mild southwesterly increase in slab dip [*Eberhart-Phillips and Reyners*, 1997].

[16] In Figure 3a, we have plotted a radial receiver function CCP stack that is perpendicular to the strike of subduction based on seismicity. We see a positive amplitude (white) receiver function arrival at 15 km depth on the left (SE) and right (NW) sides of Figure 3a, which deepens to 25 km near the center of the stack. This is underlain by a discontinuous negative amplitude (black) receiver function arrival, which varies from 25 to 50 km depth. A northwest dipping positive arrival traverses from 35 km depth in the southeast to 75 km in the northwest. Several deeper flat-lying positive and negative arrivals traverse the region.

[17] Energy on the transverse CCP stack (Figure 3b) is generally not as continuous as or well correlated with the radial CCP stack. One feature that is worth noting is the negative arrival that undulates between 20 and 35 km depths from southeast to northwest across the stack. In the southeast, this feature correlates well with a positive arrival on the radial CCP stack. In the center and northwest, this arrival does not appear to correlate with any arrivals on the radial stack.

[18] Figure 3c presents a migrated receiver function stack. The most prominent feature is a northwest dipping positive arrival, which moves from 35 km depth on the southeast side of the stack to 100 km depth on the northwest side of the stack. Paired to this arrival and confined above 50 km depth is a negative arrival. In Figure 4d, we overlay contours of seismicity for magnitudes greater than 3 within 100 km of the stack from January 2000 through March 2006 [data are available at www.geonet.org.nz]. This magnitude level appears to satisfy completeness to depths of 100 km. The aforementioned negative arrival appears to coincide with much of the dipping seismicity. Similar to the radial CCP stack, there are multiple flat-lying arrivals that are confined to the southeast section of the stack below 50 km depth.

[19] Within the horizontal extent of the station locations, migration artifacts (for example, semicircles of seismic

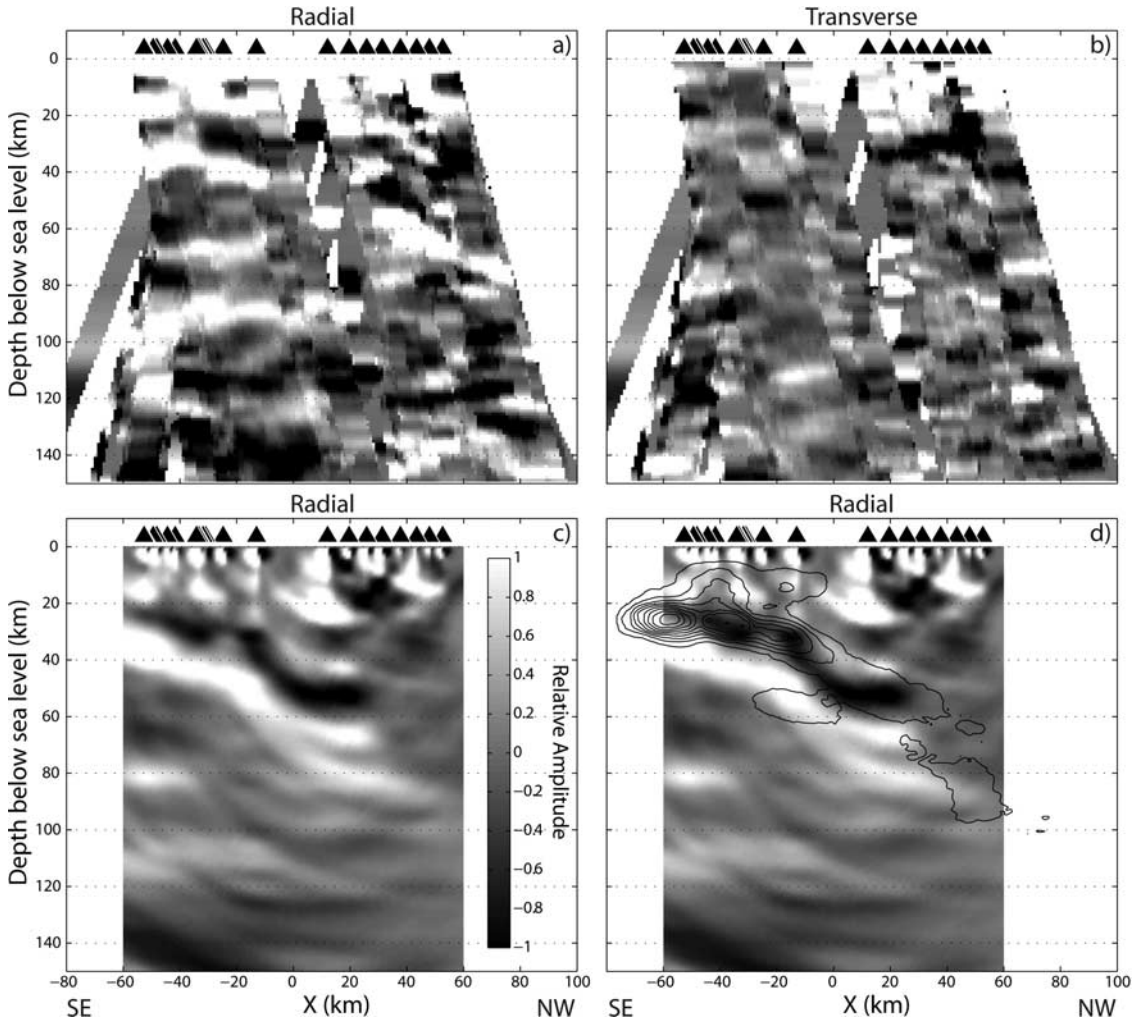

Figure 3. (a) CCP radial, (b) transverse, and (c) migrated radial receiver function stacks using teleseismic data acquired from the North and South Island stations. In Figure 3d, we overlay the migrated stack with contours of seismicity for magnitudes greater than 3 within 100 km of the stack from January 2000 through March 2006 (data are available at www.geonet.org.nz). Each contour interval represents an increase in the density of seismicity of 10%. Triangles represent station locations. Light colors are positive arrivals, which are caused by increasing velocity with depth.

energy distributed about a station) are minimal. Beyond this extent, for example at x locations near ±60 km at depths less than 20 km, arrivals curve upward as the seismic energy is smeared over a semicircle about the edge of the station coverage. Large positive and negative amplitudes within 5 km of the stations are a result of the direct P arrival present in the receiver function and the polarity correction. The vertical orientation of this energy is due to the obliquity term in the Kirchhoff migration, that is, energy arriving from directly beneath the station is given greater weight than off-axis energy.

4. Discussion

[20] A reasonable question to ask is whether the observed positive amplitude arrival at 35 km depth in the SE section of Figures 3a and 3c, which increases in dip to the NW, is associated with the subducting Pacific Plate. We have investigated this question by synthesizing receiver functions using second-order finite difference simulations [*Boyd*, 2005; *Kelly et al.*, 1976; Figure 4]. The synthetic seismograms are generated using the same distribution of raypaths as for the real North and South Island data sets, which simulates the real data going into the CCP and migrated stacks. To avoid performing time-consuming three-dimensional finite difference simulations, the raypaths for the synthetics are projected into the plane of the cross section.

[21] The finite difference model starts with the one-dimensional IASPEI91 velocity model of *Kennett and Engdahl* [1991] and is overlain by various features. In all but the first case, we impose a slab where the upper surface is dictated by seismicity [*Anderson and Webb*, 1994]. The first simulation (Figures 4a, 4b, and 4c) has only the one-dimensional velocity model, IASPEI91. In the second simulation (Figures 4d, 4e, and 4f), a slab is overlain, which has a constant velocity that is equal to IASPEI91 at 250 km depth. The third simulation has a reduced velocity in the mantle wedge dictated by a function that is Gaussian in x

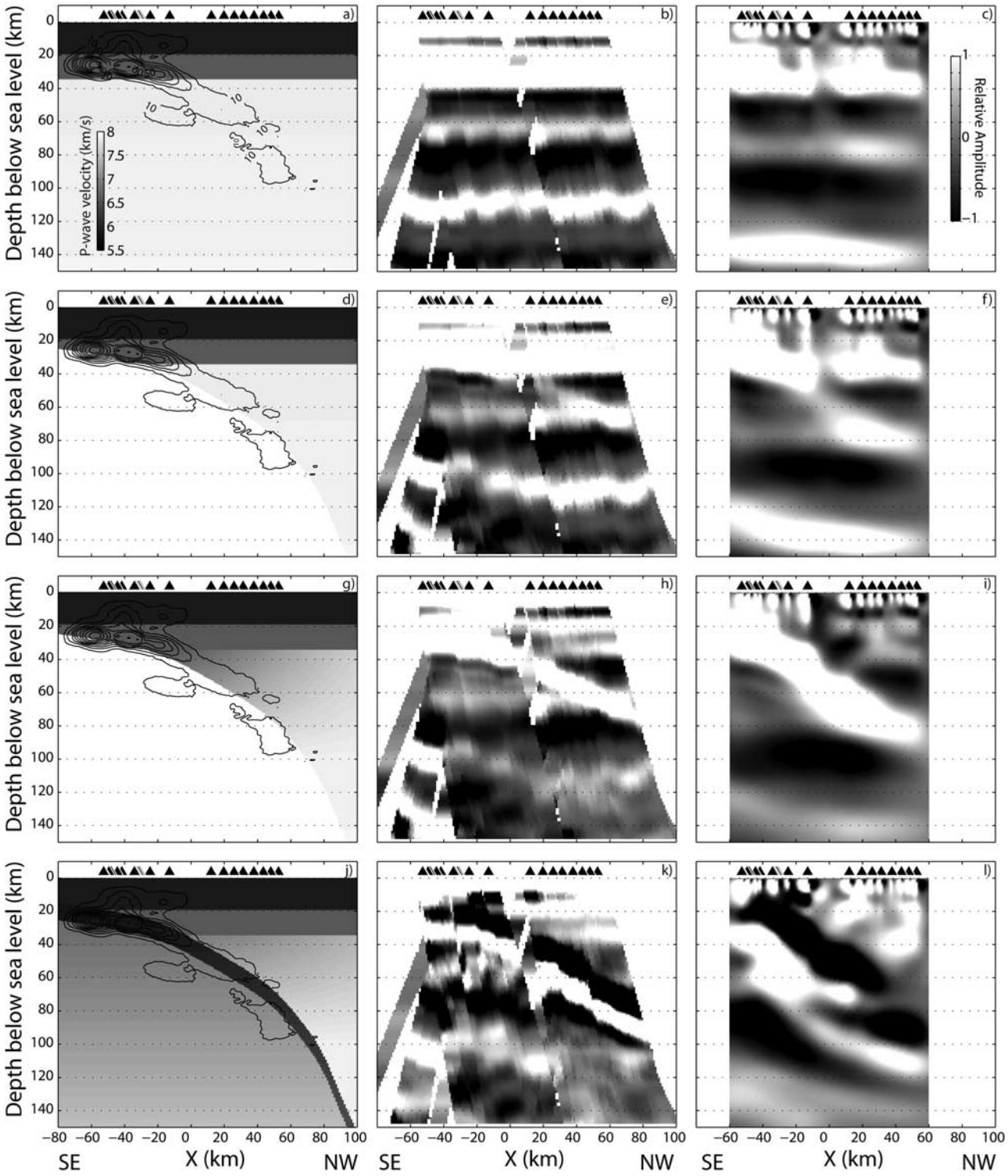

Figure 4. (b, e, h, and k) Synthetic CCP and (c, f, i, and l) migrated radial receiver function stacks for (a, d, g, and j) three earth models. In Figures 4a, 4d, 4g, and 4j, we overlay the earth model with contours of seismicity for magnitudes greater than 3 within 100 km of the stack from January 2000 through March 2006 (data are available at www.geonet.org.nz). Each contour interval represents an increase in the density of seismicity of 10% (labeled in Figure 4a). Triangles represent station locations. Light colors are positive arrivals, which are caused by increasing velocity with depth.

and linear with depth (Figures 4g, 4h, and 4i). The Gaussian has a standard deviation of 70 km, and its center lies at the intersection of the crust and subducting slab. The minimum velocity in the mantle wedge is 16% lower than the one-dimensional value. Velocities return to IASPEI91 values by 100 km depth. In the final simulation (Figures 4j, 4k, and 4l), we modify the previous parameters and add a low-velocity layer to the top of the slab. The standard deviation of the Gaussian in the mantle wedge is 100 km, and the velocity reduction is 12%. The low-velocity layer has a maximum thickness of 10 km and a velocity that increases linearly with depth. The velocity of the fast part of the slab was decreased from its value in the previous simulations in order to reduce the velocity contrast between the slow- and fast-velocity layers of the slab to a value that better reproduces the relative amplitudes in the real CCP and migrated stacks.

[22] There are several interesting consequences of these simulations. From the first simulation (Figures 4a, 4b, and 4c), we see that in the migrated stacks, gaps in station coverage produce gaps in the discontinuities, an effect which lessens with depth. We therefore expect the CCP stacks to be more reliable for imaging the continuity of shallow crustal structure and the migrated stacks to be more successful at imaging deeper structure. Surprisingly, when a high-velocity slab is overlain on the one-dimensional velocity model (Figure 4d), the slab is not exceptionally apparent in the synthetic CCP stack (Figure 4e). However, steps in velocity at 20 and 35 km depths are apparent. The weak slab conversion and strong crustal conversions are partly due to the high-velocity contrast at the Moho. On the South Island, *Wilson et al.* [2004] found two positive impedance contrasts at ~20 and 35 km depths, which, they suggest, represent the top of an anisotropic layer and the Australian Moho, respectively. In the real CCP stack (Figure 3a), we see similar arrivals at ~20 km across the entire stack and at 35 km depth intermittently, which is not entirely surprising since our South Island data set is nearly colocated with the data set of *Wilson et al.* [2004]. The negative arrival in the transverse CCP stack may be associated with an anisotropic layer observed by several authors [*Audoine et al.*, 2000; *Eberhart-Phillips and Henderson*, 2004; *Savage*, 1998; *Savage et al.*, 2007; *Wilson et al.*, 2004] and deserves further investigation in terms of anisotropic structures but is beyond the scope of this study.

[23] The large positive midcrustal arrival at 20 km depth and the potential small amplitude Moho arrival at 35 km depth between $X = 20$ and 40 km (Figure 3a) may indicate an increase in the seismic velocity of the lower crust and/or decrease in seismic velocity of the upper mantle at this particular location. NW of $X = 40$ km, the lack of a distinct positive and possible presence of a negative Moho arrival may indicate a further increase in lower crustal or a decrease in mantle wedge seismic velocity. Authors have suggested that this can be accomplished by serpentinization [*Bostock et al.*, 2002; *Park et al.*, 2004] and hydration [*Eberhart-Phillips and Reyners*, 1997] of the upper mantle. *Bostock et al.* [2002] used receiver functions and the observation of a missing continental Moho beneath Cascadia to infer the presence of a serpentinized mantle wedge. *Park et al.* [2004] also used receiver functions to infer the presence of serpentinite beneath Corvallis, Oregon, while on the north end of the South Island of New Zealand, *Eberhart-Phillips and Reyners* [1997] suggested that hydration above the subducting slab was responsible for low seismic velocities.

[24] Another notable features of the first simulation (Figures 4a, 4b, and 4c) are the *P* and *S* wave reverberations, 2P1S (positive arrival) and 2S1P (negative arrival), from the two crustal discontinuities. These traverse the entire section at depths of 70, 80, 110, and 140 km in the CCP stack and 75, 100, and 140 km in the migrated stack (2S1P for the lower crustal discontinuity is deeper than 150 km depth in the migrated section). Similar positive and negative arrivals traverse the real CCP and migrated stacks but are more apparent in the southeast. We think that these are 2P1S and 2S1P multiples from mid to lower crustal and slab-related seismic discontinuities. However, we cannot rule out that the crustal arrivals we've observed are multiples produced from shallow crustal discontinuities.

[25] The northwest dipping feature in our real data is clearly more apparent than the slab conversion in the first simulation. To bring out the slab in our simulations, we reduced the seismic impedance contrast across the bottom of the crust and increased the impedance contrast at the slab interface by reducing the seismic velocities in the mantle wedge (Figure 4g). This simulation results in a very prominent slab arrival. In the synthetic CCP stack (Figure 4h), the slab arrival increases to a maximum dip and diverges from the position of the slab expected from seismicity. This is because our receiver functions are traced back along the P_dS wave raypaths produced from a one-dimensional velocity profile, thus arrivals from dipping interfaces will not be placed in their proper subsurface position [*Chen et al.*, 2005]. When we migrate the receiver functions (Figure 4i), the slab arrival becomes steeper and coincides with seismicity southeast of $X = 60$ km. Hence, in the real CCP stack, the seismicity dips more steeply than the northwest dipping positive arrival and coincides with this arrival only at 40 km depth, while in the real migrated stack, the seismicity follows and coincides with the northwest dipping negative arrival from 30 to 70 km depth.

[26] Another feature to note in both the real and synthetic stacks is the vertical offset in slab position near $X = 0$ km. In the synthetics, this results from slab conversions coupled with the uneven distribution of stations and the large gap in station coverage. Presumably then, in the real stacks, this also results from slab conversions coupled with the uneven distribution of stations and the large gap in station coverage. However, as noted earlier, it may also be partly due to an increase in dip of the slab to the southwest.

[27] Our results are therefore consistent with a slab that bends steeply and follows observed seismicity. Relative amplitudes suggest that the true velocity contrast at the top of the slab is smaller than in our simulation and is likely smaller than the mid crustal velocity contrast. Our results also suggest that the slab extends to the southern extent of our data.

[28] In our final simulation, we introduce a low-velocity layer at the top of the slab (Figure 4j) in an attempt to reproduce some of the negative amplitude arrivals seen in the real CCP and migrated stacks. Our efforts produce a very strong set of negative and positive arrivals associated with the slab, having a very similar geometry to the results

of the second simulation. We also see additional multiple arrivals beneath the slab arrival. Some of the features associated with the low-velocity layer in our synthetics resemble features in the real CCP and migrated stacks. For example, in the real migrated stack, a prominent negative arrival is observed above the positive northwest dipping arrival. This pair of negative and positive arrivals is not seen in the simulation without a low-velocity layer. Therefore we expect that a low-velocity layer is present at the top of the subducting plate to depths of 60 km. Another interesting artifact of the processing and subsurface geometry in the migrated stacks is the double positive arrival from $X = 0$ to 20 km near 80 km depth (Figures 3c and 4i). The separation is about 30 km in the synthetic stack and only 15 km in the real migrated stack, which may indicate that our low-velocity layer is too slow and/or too thick. The effect may also be associated with reverberations in the top crustal layer, and further work would be needed to distinguish these possibilities.

[29] An inspection of the real migrated stack reveals that much of the seismicity is concentrated in the low-velocity layer. *Bourne and Stuart* [2000] studied *ScSp* precursors using broadband waveforms filtered to periods less than 10 s and suggested that a low-velocity layer was present at the top of the oceanic crust. They interpreted this layer, which they determined to be 1–2 km thick, to be very low-velocity subducted sediments lying on top of a subducting oceanic crust of 11–14 km thickness. They argued that the subducted sediment layer lies above the seismicity and deforms aseismically. A second alternative, which has been suggested by *Eberhart-Phillips and Reyners* [1997], is the dehydration of oceanic crust leading to high pore pressures, low seismic velocities, and low normal stress across faults. When we approach the transition to the mantle wedge at position $X = 0$ km, the seismicity becomes much more diffuse, possibly indicating the lack of a low-strength, hydrated, or subducted sediment layer near the top of the slab.

[30] To get the seismicity to coincide with the positive amplitude arrival would require reducing the migration *P* wave velocity to 4 km/s. Most one-dimensional seismic profiles in the region rise to 6 km/s by about 20 km depth [*Bourne and Stuart*, 2000; *Eberhart-Phillips and Reyners*, 1997; *Robinson*, 1986]. We also must consider the limited bandwidth of our data, which we have filtered to less than 1 Hz, thus we cannot be certain of the thickness of the low-velocity layer. It is likely that the low-velocity layer we consider is made up of both the low-velocity layer, possibly sediments, on top of the oceanic crust, and the crust itself, which has a lower velocity than the mantle beneath it.

5. Conclusions

[31] Our receiver function common conversion point and migrated stacks have further substantiated the location of the subducting Pacific Plate inferred from seismicity in the region of Cook Strait, New Zealand. Synthetic seismograms help us test this hypothesis and also aid in distinguishing between direct arrivals and multiples from slab and crustal structure. The subducting Pacific Plate extends to the southern extent of our stations near 42°S, contrary to recent suggestions by *Furlong* [2004]. We find a low-velocity transition at the top of the slab in the southeast and beneath the Moho in the northwest. Seismicity coincides with the negative amplitude arrival and may suggest that brittle deformation is localized in the low-velocity layer at the top of the slab. We see crustal discontinuities near 20 and 35 km depth, which are consistent with previous observations, as well as significant transverse receiver function energy, which may indicate lower crustal anisotropy, an observation also suggested by previous authors.

[32] **Acknowledgments.** We gratefully acknowledge the logistical support of T. Stern and Victoria University in Wellington, New Zealand and the fieldwork of C. Wilson, H. Gilbert, S. Bilham, D. Fee, N. Cozens, N. Daniels, C. Offutt, M. Salmon, O. Singleton, M. Duclos, and S. Toulumin for the South Island deployment. Some financial support for the South Island deployment was provided by FRST and Marsden. We acknowledge the fieldwork of G. Stuart and D. Francis and the initial processing done by H. Todd for the North Island data. The data from station SNZO were provided by IRIS. We acknowledge the New Zealand GeoNet project and its sponsors EQC, GNS, and FRST for providing earthquake locations used in this study. M. Savage acknowledges the support from a VUW Research and Study Leave grant. We thank two anonymous reviewers and an associate editor for providing thorough reviews. This study was supported by NERC grant GR3/7699 and NSF grants 9909602, 9910145, and 0106904.

References

Anderson, H., and T. Webb (1994), New Zealand seismicity: Patterns revealed by the upgraded National Seismograph Network, *N. Z. J. Geol. Geophys.*, *37*, 477–493.

Audoine, E., et al. (2000), Seismic anisotropy from local earthquakes in the transition region from a subduction to a strike-slip plate boundary, New Zealand, *J. Geophys. Res.*, *105*(B4), 8013–8034, doi:10.1029/1999JB900444.

Bostock, M. G., et al. (2001), Multiparameter two-dimensional inversion of scattered teleseismic body waves: 1. Theory for oblique incidence, *J. Geophys. Res.*, *106*, 30,771–30,782.

Bostock, M., et al. (2002), An inverted continental Moho and serpentinization of the forearc mantle, *Nature*, *417*, 536–538.

Bourne, M., and G. Stuart (2000), ScSp observed on North Island, New Zealand: implications for subducting plate structure, *Geophys. J. Int.*, *142*, 925–932.

Boyd, O. S. (2005), An efficient Matlab routine to calculate heterogeneous anisotropic wave propagation in three dimensions, *Comput. Geosci.*, *32*, 259–264.

Cande, S. C., and J. M. Stock (2004), Pacific-Antarctic-Australia motion and the formation of the Macquarie Plate, *Geophys. J. Int.*, *157*, 399–414.

Chen, L., et al. (2005), A wave equation migration method using receiver functions: II. Application to the Japan subduction zone, *J. Geophys. Res.*, *110*, B11310, doi:10.1029/2005JB003666.

Dueker, K. G., and A. F. Sheehan (1998), Mantle discontinuity structure beneath the Colorado Rocky Mountains and High Plains, *J. Geophys. Res.*, *103*, 7153–7169.

Eberhart-Phillips, D., and M. C. Henderson (2004), Including anisotropy in 3-D velocity inversion and application to Marlborough, New Zealand, *Geophys. J. Int.*, *156*, 237–254.

Eberhart-Phillips, D., and M. Reyners (1997), Continental subduction and three-dimensional crustal structure: The northern South Island, New Zealand, *J. Geophys. Res.*, *102*, 11,843–11,861.

Furlong, K. P. (2004), Making mountains along the New Zealand plate boundary: The importance of transitions and transients, *Geol. Soc. Amer. Abstr. Prog.*, *36*, 482.

Kelly, K. R., et al. (1976), Synthetic seismograms: A finite-difference approach, *Geophysics*, *41*, 2–27.

Kennett, B. L. N., and E. R. Engdahl (1991), Traveltimes for global earthquake location and phase identification, *Geophys. J. Int.*, *105*, 429–465.

Kohler, M. D., and D. Eberhart-Phillips (2002), Three-dimensional lithospheric structure below the New Zealand Southern Alps, *J. Geophys. Res.*, *107*(B10), 2225, doi:10.1029/2001JB000182.

Kohler, M. D., and D. Eberhart-Phillips (2003), Intermediate-depth earthquakes in a region of continental convergence: South Island, New Zealand, *Bull. Seismol. Soc. Am.*, *93*, 85–93.

Langston, C. A. (1977), Corvallis, Oregon, crustal and upper mantle receiver structure from teleseismic P and S waves, *Bull. Seismol. Soc. Am.*, *67*, 713–724.

Ligorria, J. P., and C. J. Ammon (1999), Iterative deconvolution and receiver-function estimation, *Bull. Seismol. Soc. Am.*, *89*, 1395–1400.

Park, J., et al. (2004), Subduction zone anisotropy beneath Corvallis, Oregon: A serpentinite skid mark of trench-parallel terrane migration?, *J. Geophys. Res.*, *109*, B10306, doi:10.1029/2003JB002718.

Reyners, M., and H. Cowan (1993), The transition from subduction to continental collision: Crustal structure in the North Canterbury region, New Zealand, *Geophys. J. Int.*, *115*, 1124–1136.

Reyners, M., and E. Robertson (2004), Intermediate depth earthquakes beneath Nelson, New Zealand, and the southwestern termination of the subducted Pacific plate, *Geophys. Res. Lett.*, *31*, L04607, doi:10.1029/2003GL019201.

Reyners, M., et al. (1997), Plate coupling in the northern South Island and southernmost North Island, New Zealand, as illuminated by earthquake focal mechanisms, *J. Geophys. Res.*, *102*, 15,197–15,210.

Robinson, R. (1986), Seismicity, structure and tectonics of the Wellington region, New Zealand, *Geophys. J. R. Astron. Soc.*, *87*, 379–409.

Savage, M. K. (1998), Lower crustal anisotropy or dipping boundaries? Effects on receiver functions and a case study in New Zealand, *J. Geophys. Res.*, *103*, 15,069–15,087.

Savage, M. K., et al. (2007), Velocity and anisotropy structure at the Hikurangi subduction margin, New Zealand from receiver functions, *Geophys. J. Int.*, *168*, 1034–1050.

Sheehan, A. F., et al. (2000), Seismic migration processing of P-SV converted phases for mantle discontinuity structure beneath the Snake River Plain, western United States, *J. Geophys. Res.*, *105*, 19,055–19,065.

Stern, T., et al. (2000), Teleseismic P wave delays and modes of shortening the mantle lithosphere beneath South Island, New Zealand, *J. Geophys. Res.*, *105*, 21,615–21,631.

Stewart, D. (1998), Earth velocity structure from an earthquake recording array, Honours thesis, Victoria University of Wellington, Wellington.

Stuart, G., et al. (1995), Tararua broadband array, North Island, New Zealand, *Bull. Seismol. Soc. Am.*, *85*, 325–333.

Wilson, C., et al. (2001), Lithospheric structure of a continental strike-slip boundary, Marlborough Fault Zone, South Island, New Zealand, *EOS Trans. AGU*, *82*, Abstract T11D-0882.

Wilson, C. K., et al. (2004), Evidence for continuous deformation in the lower crust and upper mantle beneath a continental strike-slip fault zone: Marlborough Fault System, South Island, New Zealand, *Geology*, *32*, 837–840.

Yilmaz, O. (2001), *Seismic Data Analysis,* Society of Exploration Geophysicists, Tulsa.

O. S. Boyd, C. H. Jones, and A. F. Sheehan, Department of Geological Sciences, University of Colorado at Boulder, 2200 Colorado Ave., Boulder, CO 80309-0399, USA. (oliver.boyd@colorado.edu)

M. K. Savage, Institute of Geophysics, School of Earth Sciences, Victoria University of Wellington, Wellington, New Zealand.